Order-disorder transition in a bilayer frustrated Heisenberg antiferromagnet

1999 J. Phys.: Condens. Matter 11 3175

(http://iopscience.iop.org/0953-8984/11/15/023)

J. Phys.: Condens. Matter **11** (1999) 3175–3186. Printed in the UK PII: S0953-8984(99)00322-7

Order–disorder transition in a bilayer frustrated Heisenberg antiferromagnet

Deng-Ke Yu, Qiang Gu, Han-Ting Wang and Jue-Lian Shen

Institute of Physics and Centre for Condensed Matter Physics, Chinese Academy of Sciences, PO Box 603, Beijing 100080, People's Republic of China

Received 21 December 1998, in final form 5 February 1999

Abstract. The order–disorder transition in a bilayer J_1–J_2 model (with interlayer coupling J_0) is studied by a bond-operator mean-field method. The phase diagram is obtained. On the Néel phase side, the critical interlayer coupling J_0^c decreases linearly with increasing frustration J_2 for $J_2 \leqslant 0.2J_1$ and extends down to zero at about $J_2 \simeq 0.38J_1$. On the collinear phase side, J_0^c also exhibits a linear decrease with decreasing J_2 for $J_2 \geqslant 1.0J_1$ and extends down to zero at about $J_2 \simeq 0.60J_1$. The sublattice magnetizations of both the Néel phase and the collinear phase are calculated. Near the phase boundary, we have $M \propto (J_0^c - J_0)^{1/2}$. The low-temperature quantum critical properties obtained are in agreement with those of the O(3) nonlinear σ-model.

1. Introduction

It has been suggested that the unusual normal-state magnetic properties of underdoped $YBa_2Cu_3O_{6+x}$ are due to its lying close to the zero-temperature order–disorder transition occurring in a model of two antiferromagnetically coupled planes of antiferromagnetically correlated spins (i.e., the bilayer Heisenberg antiferromagnet) [1]. Although the model captures the main physics of the material as regards its magnetic properties, the critical ratios of interlayer versus intralayer couplings that are obtained are too large ($\sim$2.5) compared with the experimental results ($\sim$0.1) [2, 3]. A realistic theory must incorporate itinerant carriers, which strongly suppress the magnetism. It has been pointed out that the magnetic effect of itinerant charge carriers can be studied by introducing frustrations into the bilayer Heisenberg antiferromagnet [4–6], since one may formally integrate out the charge degree of freedom and obtain an effective spin Hamiltonian with further-neighbour interactions [7]. We will consider here only the next-nearest-neighbour interactions for simplicity.

The two-layer, spin-1/2, frustrated Heisenberg antiferromagnet (i.e., the bilayer J_1–J_2 model) is described by

$$H = J_0 \sum_i S_{1,i} S_{2,i} + J_1 \sum_{a,\langle i,j\rangle} S_{a,i} S_{a,j} + J_2 \sum_{a,\langle i,j\rangle'} S_{a,i} S_{a,j}. \tag{1}$$

Here, $a = 1, 2$ denotes the two layers; $\langle i, j\rangle$ and $\langle i, j\rangle'$ are pairs of nearest and next-nearest neighbours in a square lattice. J_0, J_1, J_2 are all antiferromagnetic, and denote the interlayer coupling and the nearest and next-nearest intralayer couplings, respectively. The order–disorder transitions are determined by both J_0/J_1 and J_2/J_1.

Gros *et al* considered a long-range version of this model [4]. They found that the critical interlayer coupling J_0^c is reduced linearly with the in-plane frustration J_2. Dotsenko used an

0953-8984/99/153175+12$19.50

effective-action approach to study the model [5]. For values of the interlayer coupling that are not very small, the effective action of the model can be reduced to that of the quantum O(3) nonlinear σ-model (NLSM). The critical value of the interlayer coupling was found to decrease linearly with the intralayer frustration. Hida obtained a qualitative phase diagram using the modified spin-wave theory [6]. The sublattice magnetizations of both the Néel and collinear phases are calculated.

We study the bilayer J_1–J_2 model by a bond-operator mean-field method. The bond-operator representation of this model includes the longitudinal spin fluctuations [8], and mean-field theory is able to give a good description of the zero-temperature order–disorder transition and low-temperature quantum critical properties. We use the bond-operator mean-field method to compute the spectrum and spin gap of the model for the disordered phase, and the spectrum and sublattice magnetizations for the ordered phases. The phase diagram is obtained. On the Néel phase side, the critical interlayer coupling $J_0^c \simeq 2.29J_1$ at vanishing J_2 and it decreases linearly with increasing J_2 for $J_2 \leqslant 0.2J_1$. On the collinear phase side, $J_0^c \simeq 3.13J_1$ at $J_2 = 1.5J_1$ and it also exhibits a linear decrease with decreasing J_2 for $J_2 \geqslant 1.0J_1$. Extending to $J_0 = 0$, we get a nonmagnetic intermediate phase in the region $0.38J_1 < J_2 < 0.60J_1$ between the Néel phase and the collinear phase, consistent with the exact-diagonalization and series expansion results for the J_1–J_2 model [9, 10]. Near the phase boundaries in the ordered phases, the staggered and collinear magnetizations

$$M \propto (J_0^c - J_0)^{1/2}$$

indicate that the phase transitions are second order. Along the Néel phase boundary, the calculated spin-wave mass, uniform susceptibility and inverse correlation length exhibit linear behaviours versus temperature at low temperature, which are in good agreement with the O(3) NLSM predictions.

The outline of the rest of the paper is as follows. In section 2 we first introduce the bond-operator representation and then study the $T = 0$ order–disorder transition. The disordered phase, Néel phase and collinear phase are discussed. In section 3 we discuss the quantum critical properties at low temperatures. A summary is presented in section 4.

2. Order–disorder transition at zero temperature

We first introduce the bond-operator representation of quantum spins. For two $S = 1/2$ spins, $\boldsymbol{S}_1$ and $\boldsymbol{S}_2$, Sachdev and Bhatt [11] introduced four creation operators to represent the four states in Hilbert space, i.e., the singlet state $|s\rangle$ and the three triplet states $|t_x\rangle$, $|t_y\rangle$ and $|t_z\rangle$:

$$\begin{aligned}
|s\rangle &= s^\dagger|0\rangle = \frac{1}{\sqrt{2}}(|\uparrow\downarrow\rangle - |\downarrow\uparrow\rangle) \\
|t_x\rangle &= t_x^\dagger|0\rangle = \frac{-1}{\sqrt{2}}(|\uparrow\uparrow\rangle - |\downarrow\downarrow\rangle) \\
|t_y\rangle &= t_y^\dagger|0\rangle = \frac{\mathrm{i}}{\sqrt{2}}(|\uparrow\uparrow\rangle + |\downarrow\downarrow\rangle) \\
|t_z\rangle &= t_z^\dagger|0\rangle = \frac{1}{\sqrt{2}}(|\uparrow\downarrow\rangle + |\downarrow\uparrow\rangle)
\end{aligned} \tag{2}$$

where $|0\rangle$ is the vacuum state. With these definitions, $\boldsymbol{S}_1$ and $\boldsymbol{S}_2$ can be expressed as

$$\begin{aligned}
S_1^\alpha &= \frac{1}{2}(s^\dagger t_\alpha + t_\alpha^\dagger s - \mathrm{i}\epsilon_{\alpha\beta\gamma} t_\beta^\dagger t_\gamma) \\
S_2^\alpha &= \frac{1}{2}(-s^\dagger t_\alpha - t_\alpha^\dagger s - \mathrm{i}\epsilon_{\alpha\beta\gamma} t_\beta^\dagger t_\gamma)
\end{aligned} \tag{3}$$

where α, β, γ take the values x, y, z, repeated indices are summed over and ϵ is the totally antisymmetric tensor. The restriction that the physical states are either singlets or triplets leads to the constraint

$$s^\dagger s + t_\alpha^\dagger t_\alpha = 1. \tag{4}$$

The $S = 1/2$, SU(2) algebra of the spins $\boldsymbol{S}_1$ and $\boldsymbol{S}_2$ can be reproduced with s and t_α satisfying the bosonic commutation relations.

Choosing adjacent spins from the two layers as S_1 and S_2, and using the bond-operator representation [11, 12], the Hamiltonian equation (1) can be written as

$$H = H_0 + H_1 + H_2 \tag{5}$$

where

$$H_0 = \sum_i J_0\left(-\frac{3}{4}s_i^\dagger s_i + \frac{1}{4}t_{i\alpha}^\dagger t_{i\alpha}\right) - \mu_i(s_i^\dagger s_i + t_{i\alpha}^\dagger t_{i\alpha} - 1)$$

$$H_1 = \frac{J_1}{4}\sum_{i,\delta}[s_i^\dagger s_{i+\delta}^\dagger t_{i\alpha}t_{i+\delta,\alpha} + s_i^\dagger s_{i+\delta}t_{i\alpha}t_{i+\delta,\alpha}^\dagger + \text{h.c.}]$$

$$+ \frac{J_2}{4}\sum_{i,\delta'}[s_i^\dagger s_{i+\delta'}^\dagger t_{i\alpha}t_{i+\delta',\alpha} + s_i^\dagger s_{i+\delta'}t_{i\alpha}t_{i+\delta',\alpha}^\dagger + \text{h.c.}]$$

$$H_2 = \frac{J_1}{4}\sum_{i,\delta} -(1-\delta_{\alpha\beta})(t_{i\alpha}^\dagger t_{i+\delta,\alpha}^\dagger t_{i\beta}t_{i+\delta,\beta} - t_{i\alpha}^\dagger t_{i+\delta,\beta}^\dagger t_{i+\delta,\alpha}t_{i\beta})$$

$$+ \frac{J_2}{4}\sum_{i,\delta'} -(1-\delta_{\alpha\beta})(t_{i\alpha}^\dagger t_{i+\delta',\alpha}^\dagger t_{i\beta}t_{i+\delta',\beta} - t_{i\alpha}^\dagger t_{i+\delta',\beta}^\dagger t_{i+\delta',\alpha}t_{i\beta}).$$

A site-dependent chemical potential μ_i is introduced to impose the constraint of equation (4). δ and δ' denote the nearest and next-nearest neighbours.

Under the bond-operator representation of this model, the disordered and ordered phases are described as follows [11]:

(a) *The dimerized phase*. This is the magnetically disordered phase, with $\langle s\rangle \neq 0$, $\langle t_\alpha\rangle = 0$ and $\langle t_\alpha t_\beta\rangle = C\delta_{\alpha\beta}$.
(b) *The magnetically ordered phase*. Condensation of a single t_α-boson leads to long-range magnetic order, with $\langle t_\alpha\rangle \neq 0$ and $\langle s\rangle \neq 0$.

The wave vector and polarization of the mode at which the t_α-bosons condense determine the nature of the magnetic ordering.

2.1. The disordered phase

We solve the Hamiltonian of equation (5) by a mean-field approach. We take $\langle s_i\rangle = \langle s_{i+\delta}\rangle = \langle s_{i+\delta'}\rangle = \bar{s}$, and replace the local constraint μ_i by a global one μ in accordance with the translational invariance of the system. Define four mean fields P, Q, P' and Q' as

$$\begin{aligned} P &= \langle t_{i\alpha}^\dagger t_{i+\delta,\alpha}\rangle \\ Q &= \langle t_{i\alpha}^\dagger t_{i+\delta,\alpha}^\dagger\rangle \\ P' &= \langle t_{i\alpha}^\dagger t_{i+\delta',\alpha}\rangle \\ Q' &= \langle t_{i\alpha}^\dagger t_{i+\delta',\alpha}^\dagger\rangle \end{aligned} \tag{6}$$

where $\alpha = x, y, z$. In equation (6) repeated indices are not summed over. After performing a Fourier transformation of the operators

$$t_{i,\alpha} = \frac{1}{\sqrt{N}} \sum_{\boldsymbol{k}} t_{k\alpha} \mathrm{e}^{\mathrm{i}\boldsymbol{k}\cdot\boldsymbol{r}_i}$$

with N the number of dimers and $\boldsymbol{k}$ the wave vector, we obtain a mean-field Hamiltonian:

$$\begin{aligned} H_m(\mu, \bar{s}, P, Q) = N\left[\left(-\frac{3}{4}J_0 - \mu\right)\bar{s}^2 + 6J_1(Q^2 - P^2) + 6J_2(Q'^2 - P'^2) + \mu\right] \\ + \sum_{\boldsymbol{k}} \Lambda_{\boldsymbol{k}} t^{\dagger}_{k\alpha} t_{k\alpha} + \Delta_{\boldsymbol{k}}(t_{k\alpha} t_{-k\alpha} + t^{\dagger}_{k\alpha} t^{\dagger}_{-k\alpha}) \end{aligned} \tag{7}$$

with

$$\begin{aligned} \Lambda_{\boldsymbol{k}} &= \frac{J_0}{4} - \mu + 2J_1\gamma^{(1)}_{\boldsymbol{k}}(\bar{s}^2 + 2P) + 2J_2\gamma^{(2)}_{\boldsymbol{k}}(\bar{s}^2 + 2P') \\ \Delta_{\boldsymbol{k}} &= J_1\gamma^{(1)}_{\boldsymbol{k}}(\bar{s}^2 - 2Q) + J_2\gamma^{(2)}_{\boldsymbol{k}}(\bar{s}^2 - 2Q') \\ \gamma^{(1)}_{\boldsymbol{k}} &= \frac{1}{2}(\cos k_x + \cos k_y) \\ \gamma^{(2)}_{\boldsymbol{k}} &= \cos k_x \cos k_y. \end{aligned} \tag{8}$$

We diagonalize the mean-field Hamiltonian by means of a Bogoliubov transformation

$$t_{k\alpha} = u_{\boldsymbol{k}}\xi_{k\alpha} + v_{\boldsymbol{k}}\xi^{\dagger}_{-k\alpha} \tag{9}$$

where the $\xi_{k\alpha}$ are Bose operators. Then we obtain

$$\begin{aligned} H_m(\mu, \bar{s}) = N\left[\left(-\frac{3}{4}J_0\bar{s}^2 - \mu\bar{s}^2 + \mu\right) + 6J_1(Q^2 - P^2) + 6J_2(Q'^2 - P'^2)\right] \\ + \frac{3}{2}\sum_{\boldsymbol{k}}(\omega_{\boldsymbol{k}} - \Lambda_{\boldsymbol{k}}) + \sum_{\boldsymbol{k}} \omega_{\boldsymbol{k}}\xi^{\dagger}_{k\alpha}\xi_{k\alpha} \end{aligned} \tag{10}$$

with

$$\omega_{\boldsymbol{k}} = [\Lambda^2_{\boldsymbol{k}} - (2\Delta_{\boldsymbol{k}})^2]^{1/2}. \tag{11}$$

The H_2-term of equation (5) consists of four triplet t-operators, which represent higher-order fluctuations. We have checked that it makes only a small contribution to the final results. For simplicity, we just present the results without H_2; we do this by setting $P = Q = P' = Q' = 0$.

The parameters μ and $\bar{s}$ are determined by the saddle-point equations

$$\begin{aligned} \bar{s}^2 &= \frac{5}{2} - \frac{3}{N}\sum_{\boldsymbol{k}} \frac{1}{\sqrt{1 - \Gamma^2_{\boldsymbol{k}}}}\left(n_{\boldsymbol{k}} + \frac{1}{2}\right) \\ \mu &= -\frac{3}{4}J_0 + \frac{6}{N}\sum_{\boldsymbol{k}} \frac{(1 - \Gamma_{\boldsymbol{k}})(J_1\gamma^{(1)}_{\boldsymbol{k}} + J_2\gamma^{(2)}_{\boldsymbol{k}})}{\sqrt{1 - \Gamma^2_{\boldsymbol{k}}}}\left(n_{\boldsymbol{k}} + \frac{1}{2}\right) \end{aligned} \tag{12}$$

with $\Gamma_{\boldsymbol{k}} = 2\Delta_{\boldsymbol{k}}/\Lambda_{\boldsymbol{k}}$ and the Bose occupation number $n_{\boldsymbol{k}} = 1/(\exp(\omega_{\boldsymbol{k}}/T) - 1)$. At $T = 0$, we have $n_{\boldsymbol{k}} = 0$. At large enough J_0, the spectrum $\omega_{\boldsymbol{k}}$ is real and positive everywhere in the Brillouin zone. For $J_1 > 2J_2$, the band minimum is at $\boldsymbol{k} = (\pi, \pi)$. This gives the spin gap and the spin-wave velocity:

$$\begin{aligned} \Delta &= \sqrt{\left(\frac{J_0}{4} - \mu\right)\left(\frac{J_0}{4} - \mu - 4(J_1 - J_2)\bar{s}^2\right)} \\ c &= \sqrt{\left(\frac{J_0}{4} - \mu\right)(J_1 - 2J_2)\bar{s}^2}. \end{aligned} \tag{13}$$

However, for $J_1 < 2J_2$, the band minimum is at $(0, \pi)$, and the spin gap and spin-wave velocities are

$$\Delta = \sqrt{\left(\frac{J_0}{4} - \mu\right)\left(\frac{J_0}{4} - \mu - 4J_2\bar{s}^2\right)}$$
$$c_x = \sqrt{\left(\frac{J_0}{4} - \mu\right)(2J_2 - J_1)\bar{s}^2} \tag{14}$$
$$c_y = \sqrt{\left(\frac{J_0}{4} - \mu\right)(2J_2 + J_1)\bar{s}^2}$$

where C_x and C_y are spin-wave velocities on the x- and y-directions.

The spin gaps decrease with decreasing J_0 and approach zero at some particular value. The $\Delta = 0$ condition is used to determine the critical value of the interlayer coupling J_0^c. The phase diagram obtained is shown in figure 1. On the Néel phase side, $J_0^c \simeq 2.29$ for $J_2 = 0$, which is consistent with the corresponding quantum Monte Carlo (QMC) simulations and series expansion results for $J_0^c \sim 2.5$ [13–16]. The critical interlayer coupling J_0^c decreases linearly with the in-plane frustration J_2 for $J_2 \leqslant 0.2J_1$, while for $J_2 > 0.2J_1$, J_0^c goes down more sharply to zero at about $J_2 \simeq 0.38J_1$. This is in agreement with the effective-action approach that finds a linear decrease of J_0^c with increase of J_2 for J_0^c not very small [5]. On the collinear phase side, we get $J_0^c \simeq 3.13J_1$ for $J_2 = 1.5J_1$, about half of the value obtained from modified spin-wave theory [6]. Similarly, J_0^c decreases linearly with decreasing J_2 for $J_2 \geqslant 1.0J_1$ and approaches zero at about $J_2 \simeq 0.60J_1$.

It has been shown that in the single-layer J_1–J_2 model there exists a nonmagnetic intermediate phase in the parameter region $0.4J_1 < J_2 < 0.6J_1$ between the Néel and collinear phases [9, 10]. Interestingly enough, our calculations with J_0 extending to zero show that the intermediate phase lies in the region $0.38J_1 < J_2 < 0.60J_1$, in agreement with the exact results. The reliability of the result depends on the magnitude of $\bar{s}^2$. In our self-consistent

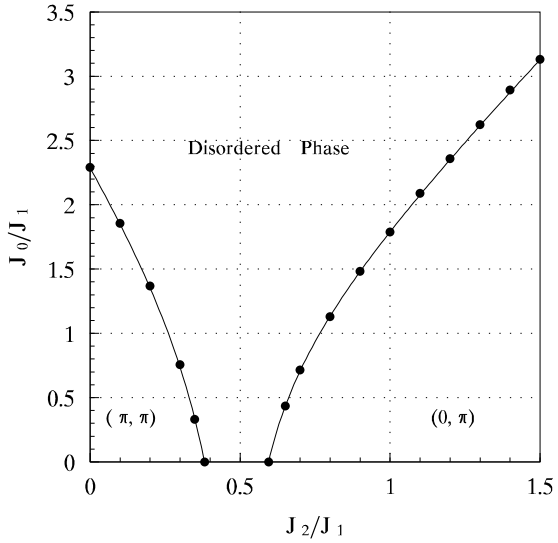

Figure 1. The phase diagram of the bilayer J_1–J_2 model. Dots and curves are results obtained for the disordered phase and ordered phases, respectively.

calculations, we get $\bar{s}^2 \sim 0.5$ at the critical points for $J_0 = 0$ ($J_2^c \simeq 0.38J_1$ on the Néel phase side and $J_2^c \simeq 0.60J_1$ on the collinear phase side), which is not very small compared with $\bar{s}^2 \sim 0.8$ at the critical point of $J_2 = 0$ ($J_0^c \simeq 2.29J_1$).

2.2. The Néel ordered phase

To describe the Néel ordered phase, we condense the t_z-operator for momentum $\boldsymbol{k}_0 = (\pi, \pi)$, with $t_{kz} = \bar{t}\delta_{k,k_0} + \tilde{t}_{kz}$. The Hamiltonian can be written as

$$H_m(\mu, \bar{s}, \bar{t}) = NE_0 + \sum_{\boldsymbol{k}}[\Lambda_{\boldsymbol{k}}(t^\dagger_{\boldsymbol{k}\alpha}t_{\boldsymbol{k}\alpha} + \tilde{t}^\dagger_{\boldsymbol{k}z}\tilde{t}_{\boldsymbol{k}z}) + \Delta_{\boldsymbol{k}}(t_{\boldsymbol{k}\alpha}t_{-\boldsymbol{k}\alpha} + t^\dagger_{\boldsymbol{k}\alpha}t^\dagger_{-\boldsymbol{k}\alpha} + \tilde{t}_{\boldsymbol{k}z}\tilde{t}_{-\boldsymbol{k}z} + \tilde{t}^\dagger_{\boldsymbol{k}z}\tilde{t}^\dagger_{-\boldsymbol{k}z})] \tag{15}$$

with

$$E_0 = \left(-\frac{3}{4}J_0 - \mu\right)\bar{s}^2 + \left(\frac{J_0}{4} - \mu\right)\bar{t}^{\,2} - 4(J_1 - J_2)\bar{s}^2\bar{t}^{\,2} + \mu. \tag{16}$$

The $\Lambda_{\boldsymbol{k}}$ and $\Delta_{\boldsymbol{k}}$ are given by equation (8), but setting $P = Q = P' = Q' = 0$, $\alpha = x, y$, $\boldsymbol{k} \neq \boldsymbol{k}_0$ in the summation over z terms. Equation (15) can be diagonalized as follows:

$$H_m(\mu, \bar{s}, \bar{t}) = NE_0 + \frac{3}{2}\sum_{\boldsymbol{k}}(\omega_{\boldsymbol{k}} - \Lambda_{\boldsymbol{k}}) + \sum_{\boldsymbol{k}}\omega_{\boldsymbol{k}}(\xi^\dagger_{\boldsymbol{k}\alpha}\xi_{\boldsymbol{k}\alpha} + \tilde{\eta}^\dagger_{\boldsymbol{k}}\tilde{\eta}_{\boldsymbol{k}}) \tag{17}$$

where

$$\omega_{\boldsymbol{k}} = \sqrt{\left(\frac{J_0}{4} - \mu\right)\left(\frac{J_0}{4} - \mu + 4\bar{s}^2(J_1\gamma^{(1)}_{\boldsymbol{k}} + J_2\gamma^{(2)}_{\boldsymbol{k}})\right)}$$

has the same form as in the disordered phase. $\xi^\dagger_{\boldsymbol{k}\alpha}\xi_{\boldsymbol{k}\alpha}$ are the transverse modes; $\tilde{\eta}^\dagger_{\boldsymbol{k}}\tilde{\eta}_{\boldsymbol{k}}$ is the longitudinal mode, which is neglected by the spin-wave theory. Equation (17) shows that the transverse modes and longitudinal mode are degenerate. This degeneracy may be lifted by including H_2.

The saddle-point equation $\langle \partial H_m/\partial \bar{t}\,\rangle = 0$ yields

$$\mu = \frac{J_0}{4} - 4(J_1 - J_2)\bar{s}^2 \tag{18}$$

which makes the excitation spectrum gapless, with

$$\omega_{\boldsymbol{k}} = 4(J_1 - J_2)\bar{s}^2\sqrt{1 + \frac{J_1\gamma^{(1)}_{\boldsymbol{k}} + J_2\gamma^{(2)}_{\boldsymbol{k}}}{J_1 - J_2}}. \tag{19}$$

A nonvanishing $\bar{t}$ indicates the existence of long-range order, with the sublattice magnetization

$$M = \frac{1}{2}\langle S_{1z} - S_{2z}\rangle = \sqrt{\bar{s}^2\bar{t}^{\,2}}.$$

Self-consistent equations for $\bar{s}$ and $\bar{t}$ at $T = 0$ are obtained from $\langle \partial H_m/\partial \mu\rangle = 0$ and $\langle \partial H_m/\partial \bar{s}\rangle = 0$:

$$\begin{aligned} &\bar{s}^2 + \bar{t}^{\,2} = Z_1 \\ &\bar{s}^2 - \bar{t}^{\,2} = \frac{J_0}{4(J_1 - J_2)} + Z_2 \end{aligned} \tag{20}$$

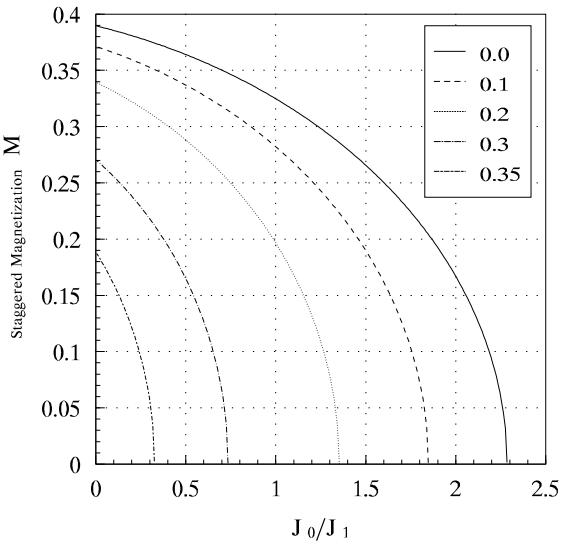

Figure 2. Staggered magnetizations of the Néel phase with various values of J_2.

with

$$Z_1 = \frac{5}{2} - \frac{3}{2N}\sum_{\boldsymbol{k}} \frac{1}{\sqrt{1-\Gamma_{\boldsymbol{k}}^2}}$$
$$Z_2 = -\frac{3}{4N}\frac{1}{J_1 - J_2}\sum_{\boldsymbol{k}} \frac{(1-\Gamma_{\boldsymbol{k}})(J_1\gamma_{\boldsymbol{k}}^{(1)} + J_2\gamma_{\boldsymbol{k}}^{(2)})}{\sqrt{1-\Gamma_{\boldsymbol{k}}^2}} \tag{21}$$
$$\Gamma_{\boldsymbol{k}} = \frac{J_1\gamma_{\boldsymbol{k}}^{(1)} + J_2\gamma_{\boldsymbol{k}}^{(2)}}{2(J_1 - J_2) + J_1\gamma_{\boldsymbol{k}}^{(1)} + J_2\gamma_{\boldsymbol{k}}^{(2)}}.$$

The parameters Z_1 and Z_2 are determined by J_1 and J_2 only, and can be directly calculated. We obtain

$$M = \frac{1}{2}\sqrt{\left[\frac{J_0}{4(J_1 - J_2)} + (Z_1 + Z_2)\right]\left[-\frac{J_0}{4(J_1 - J_2)} + (Z_1 - Z_2)\right]}. \tag{22}$$

By setting $M = 0$, we get the critical value $J_0^c = 4(J_1 - J_2)(Z_1 - Z_2)$, which is the same as that obtained from the disordered phase. The phase transition is second order. Near the critical point, $M \propto (J_0^c - J_0)^{1/2}$. The staggered magnetizations with various values of J_2 are shown in figure 2. In general, the frustration J_2 suppresses the long-range Néel order. Spin-wave theory [6, 17] and other methods [8, 16, 18] show that a small J_0 will make the system more 'classical', and only at larger J_0 do quantum fluctuations push the system towards the disordering transition. We cannot observe this because the magnetization obtained drops monotonically with J_0. At $J_0 = 0$, the sublattice magnetizations obtained are somewhat larger than those obtained from the single-layer J_1–J_2 model [10].

2.3. The collinear ordered phase

To describe the collinear ordered phase, we condense the t_{kz}-operator for momentum $\boldsymbol{k}_0 = (0, \pi)$, with $t_{kz} = \bar{t}\delta_{k,k_0} + \tilde{t}_{kz}$. The Hamiltonian has the same form of equation (15) as in the

Néel phase, but with E_0 given by

$$E_0 = \left(-\frac{3}{4}J_0 - \mu\right)\bar{s}^2 + \left(\frac{J_0}{4} - \mu\right)\bar{t}^{\,2} - 4J_2\bar{s}^2\bar{t}^{\,2} + \mu. \tag{23}$$

The saddle-point equation $\langle \partial H_m/\partial \bar{t}\,\rangle = 0$ yields

$$\mu = \frac{J_0}{4} - 4J_2\bar{s}^2. \tag{24}$$

Similarly, the saddle-point equation for $\bar{t}$ makes the excitation spectrum gapless, with

$$\omega_k = 4J_2\bar{s}^2\sqrt{1 + \frac{J_1\gamma_k^{(1)} + J_2\gamma_k^{(2)}}{J_2}}. \tag{25}$$

The long-range order sets in with a nonvanishing $\bar{t}$. The transverse modes and longitudinal mode are also degenerate. Self-consistent equations for $\bar{s}$ and $\bar{t}$ at $T = 0$ are

$$\begin{aligned} \bar{s}^2 + \bar{t}^{\,2} &= Z_3 \\ \bar{s}^2 - \bar{t}^{\,2} &= \frac{J_0}{4J_2} + Z_4 \end{aligned} \tag{26}$$

with

$$\begin{aligned} Z_3 &= \frac{5}{2} - \frac{3}{2N}\sum_k \frac{1}{\sqrt{1-\Gamma_k^2}} \\ Z_4 &= -\frac{3}{4N}\frac{1}{J_2}\sum_k \frac{(1-\Gamma_k)(J_1\gamma_k^{(1)} + J_2\gamma_k^{(2)})}{\sqrt{1-\Gamma_k^2}} \\ \Gamma_k &= \frac{J_1\gamma_k^{(1)} + J_2\gamma_k^{(2)}}{2J_2 + J_1\gamma_k^{(1)} + J_2\gamma_k^{(2)}}. \end{aligned} \tag{27}$$

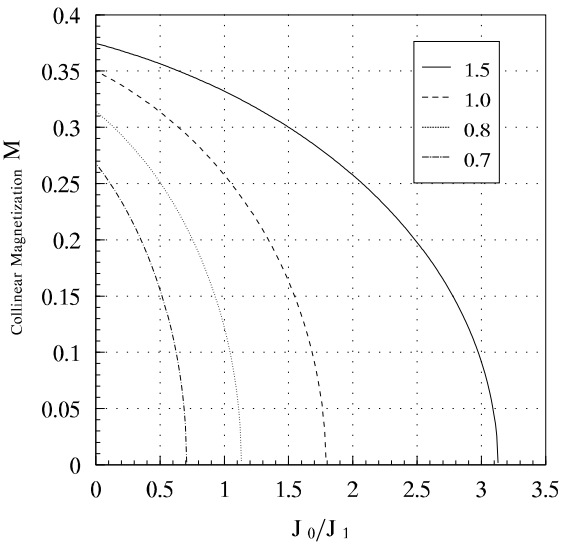

Figure 3. Collinear magnetizations of the collinear phase with various values of J_2.

The parameters Z_3 and Z_4 can be directly calculated. We obtain

$$M = \frac{1}{2}\sqrt{\left[\frac{J_0}{4J_2} + (Z_3 + Z_4)\right]\left[-\frac{J_0}{4J_2} + (Z_3 - Z_4)\right]}. \tag{28}$$

The critical value $J_0^c = 4J_2(Z_1 - Z_2)$ is also the same as that obtained from the disordered phase. The phase transition is also second order, with $M \propto (J_0^c - J_0)^{1/2}$ near the phase boundary. The collinear magnetizations with various J_2 are shown in figure 3.

In general, spin-wave theories neglect longitudinal spin fluctuations and can yield reliable results only at small J_0/J_1; the bond-operator mean-field theory is appropriate near the transition point, but cannot give accurate results in the small-J_0/J_1 limit.

3. Quantum critical behaviour at low temperatures

We now discuss the low-temperature quantum critical properties for systems exactly at critical points. The QMC simulations have shown that the critical properties of the (unfrustrated) bilayer Heisenberg antiferromagnet are in good agreement with those of the O(3) NLSM [19]. For the bilayer frustrated Heisenberg antiferromagnet, it was shown that the effective action derived from the microscopic Hamiltonian has the form of the O(3) NLSM for interlayer couplings that are not very small. It is therefore reasonable that the critical properties of the bilayer frustrated antiferromagnet are also described by the O(3) NLSM for those interlayer couplings.

At finite temperatures, the systems are still described by the self-consistent equations (12). We set the systems exactly at the critical points and set $J_1 = 1$.

The $1/N$ expansions of the NLSM predict that the spin-wave mass is a linear function of temperature: $m = 1.04T$ [19]. QMC simulations for the (unfrustrated) bilayer Heisenberg antiferromagnet give $m = 1.02T$ [13]. In our calculations, the spin-wave mass is given by equation (13) on the Néel phase side and by equation (14) on the collinear phase side. We find that the spin-wave masses show good linear behaviour versus temperature at low temperatures. In the temperature region $T \leqslant 0.3J_1$, we get on the Néel phase side $m/T = 0.983, 0.993, 1.009, 1.035, 1.062$ for $J_2 = 0.0, 0.1, 0.2, 0.3, 0.372$, respectively. The spin-wave mass on the collinear phase side is similar. At low temperatures, we have $m/T = 0.976, 0.992, 1.020$ for $J_2 = 1.5, 1.0, 0.8$ respectively. At low temperatures, the spin-wave velocities retain their $T = 0$ values. At higher temperatures, they drop with temperature.

The uniform susceptibility per chemical unit cell is defined as [13]

$$\chi_u = \frac{1}{NT}\sum_{ij}\langle(S^z_{1,i} + S^z_{2,i})(S^z_{1,j} + S^z_{2,j})\rangle.$$

Replacing $S^z_{n,i}$ and $S^z_{n,j}$ ($n = 1, 2$) with the bond operators and using a procedure similar to that used in modified spin-wave theory [20], we get

$$\chi_u = \frac{2}{NT}\sum_{\boldsymbol{k}} n_{\boldsymbol{k}}(n_{\boldsymbol{k}} + 1)$$

where $n_{\boldsymbol{k}}$ is the Bose occupation number. As is shown in figure 4, the uniform susceptibility also exhibits linear behaviour at low temperatures. The uniform magnetic susceptibility given by the NLSM [19] is

$$\chi_u = \frac{\sqrt{5}}{\pi c^2}\ln\left(\frac{\sqrt{5}+1}{2}\right)\left(\frac{8\pi}{15}\rho_s + 0.7937T\right) \tag{29}$$

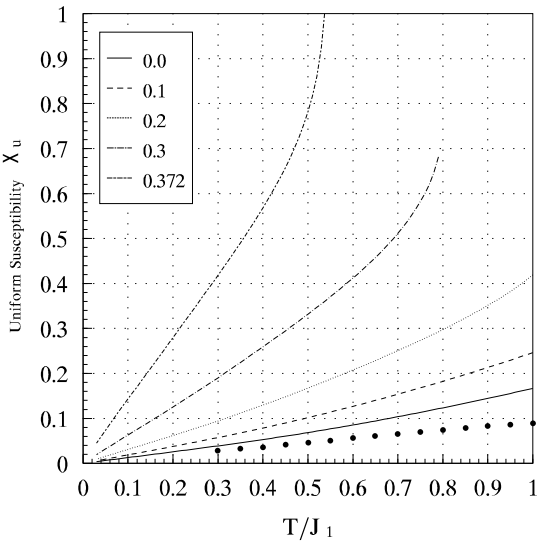

Figure 4. Uniform susceptibility versus temperature at the critical points with various values of J_2. Solid circles show the QMC results for the $J_2 = 0$ case [13].

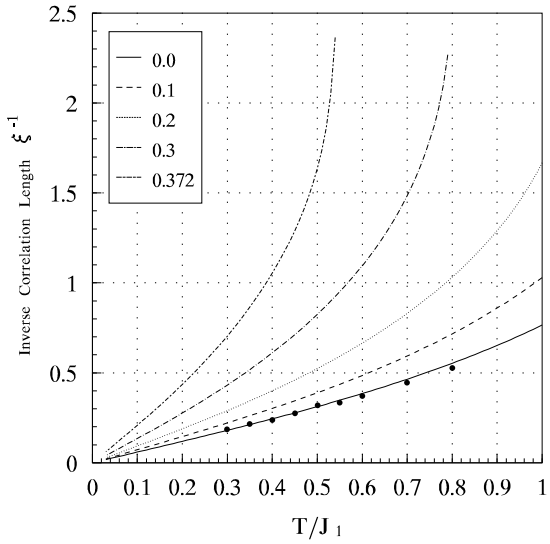

Figure 5. Inverse correlation length versus temperature at the critical points with various values of J_2. Solid circles show the QMC results for the $J_2 = 0$ case [13].

with c the spin-wave velocity and ρ_s the spin stiffness. At the critical point, where $\rho_s = 0$, we should have $\chi_u \propto T$. Fitting equation (29) in the temperature region $T \leqslant 0.3J_1$, we get

$$\chi_u \simeq C_\chi \frac{\sqrt{5}}{\pi c^2} \ln\left(\frac{\sqrt{5}+1}{2}\right) T \tag{30}$$

with $C_\chi = 1.011, 1.010, 1.004, 0.979, 0.909$ for $J_2 = 0.0, 0.1, 0.2, 0.3, 0.372$, respectively. The coefficient C_χ remains approximately constant for varying J_2 and does not deviate far from the NLSM result of 0.7937.

The NLSM prediction for the inverse correlation length is also a linear function of the temperature [19]:

$$\xi^{-1} = 1.0791 \times 2\ln\left(\frac{\sqrt{5}+1}{2}\right)\frac{T}{c} - \frac{4\pi\rho_s}{3\sqrt{5}c}. \tag{31}$$

Exactly at the critical point, $\xi^{-1} \propto T$. We extract ξ from the correlation function $\langle S^z_{1i} S^z_{1j}\rangle$ [13] and get

$$\xi^{-1} = m/c.$$

As shown in figure 5, the inverse correlation length obtained also maintains good linear behaviour at low temperatures. Fitting equation (31) in the temperature region $T \leqslant 0.3J_1$, we get

$$\xi^{-1} \simeq C_\xi \times 2\ln\left(\frac{\sqrt{5}+1}{2}\right)\frac{T}{c} \tag{32}$$

with $C_\xi = 1.023, 1.035, 1.055, 1.094, 1.165$ for $J_2 = 0.0, 0.1, 0.2, 0.3, 0.372$ respectively. C_ξ remains constant for varying J_2 and is in good agreement with that from NLSM predictions.

4. Summary

In this paper we have studied the bilayer frustrated Heisenberg antiferromagnet using a bond-operator mean-field method. This method takes into account the longitudinal spin fluctuations neglected by spin-wave theories; therefore it is able to give a more reasonable description of the zero-temperature order–disorder transition and the low-temperature quantum critical properties. A phase diagram is obtained. On the Néel phase side, the critical interlayer coupling J_0^c decreases linearly with increasing frustration J_2 for $J_2 \leqslant 0.2J_1$ and extends down to zero at about $J_2 \simeq 0.38J_1$. On the collinear phase side, J_0^c also exhibits a linear decrease with decreasing J_2 for $J_2 \geqslant 1.0J_1$ and extends down to zero at about $J_2 \simeq 0.60J_1$. The sublattice magnetizations of both the Néel phase and the collinear phase are calculated. Near the phase boundary, we have $M \propto (J_0^c - J_0)^{1/2}$. Along the Néel phase boundary, the calculated spin-wave mass, uniform susceptibility and inverse correlation length exhibit linear behaviour versus temperature at low temperatures, in good agreement with the O(3) nonlinear σ-model predictions.

References

[1] Millis A J and Monien H 1993 *Phys. Rev. Lett.* **70** 2810
Millis A J and Monien H 1994 *Phys. Rev.* B **50** 16 606
[2] Reznik D, Bourges P, Fong H F, Regnault L P, Bossy J, Vettier C, Milius D L, Aksay I A and Keimer B 1996 *Phys. Rev.* B **53** R14 741
[3] Hayden S M, Aeppli G, Perring T G, Mook H A and Doğan F 1996 *Phys. Rev.* B **54** R6905
[4] Gros C, Wenzel W and Richter J 1995 *Europhys. Lett.* **32** 747
[5] Dotsenko A V 1995 *Phys. Rev.* B **52** 9170
[6] Hida K 1996 *J. Phys. Soc. Japan* **65** 594
[7] Inui M, Doniach S and Gabay M 1988 *Phys. Rev.* B **38** 6631
[8] Chubukov A V and Morr D K 1995 *Phys. Rev.* B **52** 3521
[9] Einarsson T and Schulz H J 1995 *Phys. Rev.* B **51** 6151
[10] Oitmaa J and Zheng Weihong 1996 *Phys. Rev.* B **54** 3022
[11] Sachdev S and Bhatt R N 1990 *Phys. Rev.* B **41** 9323
[12] Gopalan S, Rice T M and Sigrist M 1994 *Phys. Rev.* B **49** 8901
[13] Sandvik A W and Scalapino D J 1994 *Phys. Rev. Lett.* **72** 2777
Sandvik A W, Chubukov A V and Sachdev S 1995 *Phys. Rev.* B **51** 16 483

[14] Hida K 1992 *J. Phys. Soc. Japan* **61** 1013
[15] Gelfand M P 1996 *Phys. Rev.* B **53** 11 309
[16] Zheng Weihong 1997 *Phys. Rev.* B **55** 12 267
[17] Ng K K, Zhang F C and Ma M 1996 *Phys. Rev.* B **53** 12 196
[18] Sandvik A W and Scalapino D J 1996 *Phys. Rev.* B **53** R526
[19] Chubukov A V and Sachdev S 1993 *Phys. Rev. Lett.* **71** 169
Chubukov A V, Sachdev S and Ye J 1994 *Phys. Rev.* B **49** 11 919
van Duin C N A and Zaanen J 1997 *Phys. Rev. Lett.* **78** 3019
Chakravarty S, Halperin B I and Nelson D R 1988 *Phys. Rev. Lett.* **60** 1057
[20] Takahashi M 1989 *Phys. Rev.* B **40** 2494